Electronic Structure, Spin-States, and Spin-Crossover Reaction of Heme-Related Fe-Porphyrins: A Theoretical Perspective

ARTICLE *in* THE JOURNAL OF PHYSICAL CHEMISTRY B · APRIL 2012

Impact Factor: 3.3 · DOI: 10.1021/jp3021563 · Source: PubMed

3 AUTHORS:

Md. Ehesan Ali
Institute of Nano Science and Technology
26 PUBLICATIONS **515** CITATIONS
SEE PROFILE

Biplab Sanyal
Uppsala University
239 PUBLICATIONS **3,285** CITATIONS
SEE PROFILE

Peter M. Oppeneer
Uppsala University
315 PUBLICATIONS **4,800** CITATIONS
SEE PROFILE

THE JOURNAL OF PHYSICAL CHEMISTRY B

Article

pubs.acs.org/JPCB

Electronic Structure, Spin-States, and Spin-Crossover Reaction of Heme-Related Fe-Porphyrins: A Theoretical Perspective

Md. Ehesan Ali*

Centre for Theoretical Chemistry, Ruhr-Universität, D-44780 Bochum, Germany

Biplab Sanyal and Peter M. Oppeneer

Department of Physics and Astronomy, Uppsala University, Box 516, S-751 20 Uppsala, Sweden

ABSTRACT: The electronic structures, spin-states, and geometrical parameters of tetra-, penta-, and hexa-coordinated iron-porphyrins are investigated applying density functional theory (DFT) based calculations, utilizing the plane-wave pseudopotential as well as localized basis set approaches. The splitting of the spin multiplet energies are investigated applying various functionals including recently developed hybrid meta-GGA (M06 family) functionals. Almost all of the hybrid functionals accurately reproduce the experimental ground state spins of the investigated Fe-porphyrins. However, the energetic ordering of the spin-states and the energies between them are still an issue. The widely used B3LYP provides consistent results for all chosen systems. The GGA+U functionals are found to be equally competent. After assessing the performance of various functionals in spin-state calculations, the potential energy surfaces of the oxygen binding process by heme is investigated. This reveals a "double spin-crossover" feature for the lowest energy reaction path that is consistent with previous CASPT2 calculations but predicting a lowest energy singlet state. The calculations have hence captured the spin-crossover as well as spin-flip processes. These are driven by the intra-atomic orbital polarization on the central metal atom due to the atomic and orbitals rearrangements. The nature of the chemical bonding and a molecular orbital analysis are also performed for the geometrically simple but electronic structurally complicated system tetra-coordinated planar Fe porphyrin in comparison to the penta-coordinated systems. This analysis explains the observed paradoxical appearance of certain peaks in the local density of states (DOS).

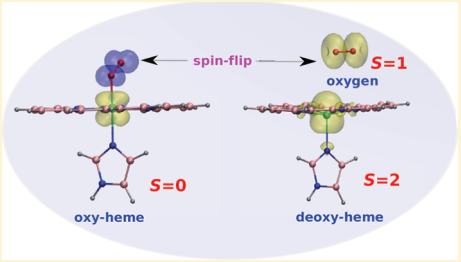

1. INTRODUCTION

Porphyrin molecules serve as active centers in metalloproteins and take part in numerous enzymatic as well as biologically relevant reactions.[1−4] One of the most important examples is the oxygen transportation by hemoglobin (an iron porphyrin complex embedded in the globin protein) to each living cell in a mammalian's body.[5,6] Photoenergy harvesting by chlorophyl during the photosynthesis process is another important example. Apart from these functionalities, porphyrin molecules have recently been used as spintronic building blocks because of their proficient nature of self-assembling as well as controlled magnetic properties upon dedicated fabrications.[7−10] Porphyrin molecules are also promising candidates as dye for solar cells.[11] The highest occupied molecular orbitals (HOMOs) of the prophyrin systems reside between the valence and conductance band of semiconductor materials upon which these are deposited. This facilitates the photoexcitation as the band gap between the HOMO of the dye and conductance band of the substrate is lowered and thereby corresponds to the visible range of photoenergies.

The origin of the interesting physical properties relevant for technological applications is the partial occupancy of the d frontier orbitals of the central metal atom, which are also responsible for various chemical reactions. A complete understanding of the electronic structure of metalloporphyrin systems at a quantitative level is, however, far from being achieved. The open d-shell allows for various possible electronic configurations and can support different spin-multiplets (low spin, intermediate, and high-spin states), which can give rise to spin-crossover behavior. The spin-multiplet energetics of nearly degenerate spin-states in metalloporphyrin systems is a topic of ongoing research and is also a challenge from the theoretical perspective. In this context, the wave function based approaches such as CASSCF, CAS-CI, CASPT2, and CCSD(T) are in principle the preferential choices of methods to be used. It has been realized that the theoretical approach which considers both dynamical and nondynamical electron correlation effects is most suitable for studying these complex systems.[14] However, the muticonfigurational approaches are restricted by the system size due to the huge computational costs even for a rather limited active space.

On the other hand, the DFT-based methods have become more useful, in the first place, because of their conceptual

Received: March 5, 2012
Revised: April 17, 2012
Published: April 18, 2012

simplicity as well as the computational perspective these methods offer for simulations of large systems (e.g., metal−organic molecule−surface interactions). The ample amount of previous theoretical works on metalloporphyrin exemplifies that the domain of density functional theory is mostly challenged particularly regarding the quantitative description of nearly degenerate spin-states.[15−18] In spite of the existing difficulty in predicting correctly the spin-state, DFT, even at the generalized gradient approximation (GGA) level, could successfully predict the structural properties for most of the investigated systems.[19−24] Conversely, the spin-states energetics of metalloporphyrin complexes are controlled by various influences, such as the nature of the axial ligands, coordination symmetry, crystal field, and the redox state of the central transition-metal atom. The general failure of the DFT at the GGA level to accurately reproduce the electronic structures of metalloporphyrin complexes has been attributed to the presence of low-lying accessible spin-states, leading to a wrong order of spin-multiplet energies.[16−18] Apart form this system-specific problem, DFT inherently suffers from the self-interaction errors which artificially delocalize the d-orbitals of transition-metal atoms.[25,26] In this context a few approaches have been developed in parallel to tackle the self-interaction problem, such as the inclusion of nonlocal exchange in the hybrid functionals or the inclusion of the on-site Coulomb correction in the GGA+U methodology.[27,28] Also more rigorous methods existing in the literature, such as the SIC correction for all the occupied orbitals,[29] the ensemble averaged restricted open-shell (ROKS) approach etc.[30]

In this work we systematically investigate and compare the ground-state spin and the energetics of the various low-lying spin-multiplets in the hybrid functional framework as well as GGA+U approach for tetra-coordinated Fe-porphyrin (abbreviated **FeP**), three penta-coordinated Fe-porphyrin molecules, viz. with a chloride ligand (**FePCl**), a hydroxyl ligand (**FePOH**), and an imidazole ring ligand (**FePIm**), and one hexa-coordinated porphyrin ligated with both an imidazole ring and an O_2 group (**FePImO2**). The latter two systems contain the functional Fe porphyrin groups of deoxyhemoglobin and oxyhemoglobin, whereas the FePCl and FePOH contain the main functional parts of hemin and hematin, respectively. After a systematic assessment of the performance of the various DFT functionals, we will explore the potential energy curve for the "spin-crossover" oxygen binding process FePIm + O_2 ⇌ $FePImO_2$ reaction and nature of the Fe−O chemical bonding. Finally, a discussion on the nature of metal−ligand bonding for iron-porphyrin complexes will be provided.

II. COMPUTATIONAL METHODS

In heme the iron-protoporphyrin contains four methyl groups, two vinylic groups and two propionic acid groups in the side chain. These side chains are replaced here by the appropriate number of hydrogen atoms to reduce the system size of the metalloporphyrin model systems to a reasonable one. The central transition metal atom dominates the interesting chemical and physical properties of the porphyrin species and such truncated macromolecular model system can reproduce these properties with a tractable amount of computational resources. This has experienced by various researchers.[15−24] The proximal histidine residues are mimicked by the imidazole subunit that occupies the fifth coordination position of **FePIm** and **FePImO2**. The molecular geometries for all the species are fully optimized with an atom centered localized Gaussian basis set approach, employing the hybrid functional (B3LYP), as well as a plane wave pseudopotential approach with an on-site Coulomb U correction (i.e., GGA+U method).

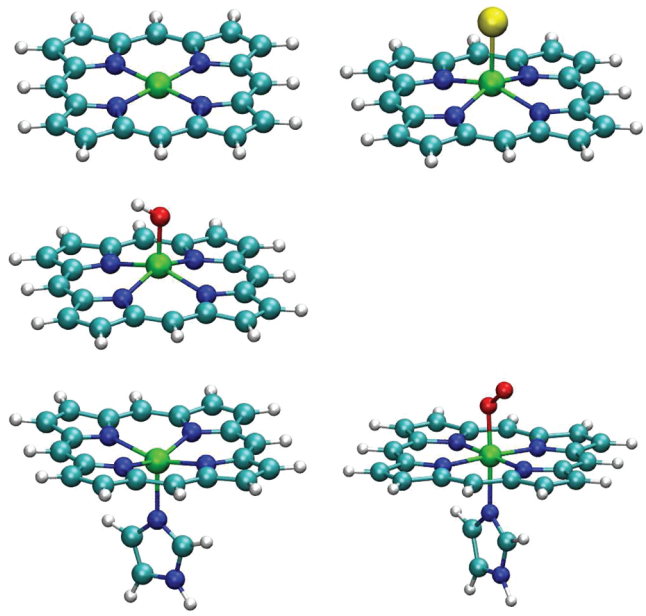

Figure 1. Optimized molecular structures of the metalloporphyrins considered in the present work. From top to bottom: Fe porphyrin (FeP), chloride ligated FeP (FePCl), hydroxyl ligated FeP (FePOH), imidazole ligated (FePIm), and imidazole and O_2 ligated (FePImO2). Nitrogen atoms are shown in dark blue, carbon in cyan, iron in green, hydrogen in white, clorine in yellow, and oxygen in red.

The single-point energy calculations are performed with the all-electron localized basis sets including diffusion function, 6-311+G(d,p), without any pseudopotential for the inner core Fe-orbitals. However, the 6-311G(d,p) basis sets are used for the lighter elements (Cl, O, N, C and H) and LANL2dz basis set is used for the Fe atom (with LANL2 pseudopotential for the 10 inner core−electrons) during the geometry optimization.[31] The localized basis sets calculations are performed using the *Gaussian 09* quantum chemistry code.[32] The plane wave calculations with GGA+U functionals are performed using kinetic energy cut off of 400 eV in projector augmented wave (PAW) method[33] with PW91 exchange-correlation functionals.[34] The PAW calculations are performed using VASP4.6.[35,36] The chosen values for the Hubbard-U and exchange J parameters are 4 and 1.0 eV, respectively (see, e.g., refs 16 and 17).

In the localized basis sets approach, the geometry optimizations were followed by an analytical second derivative calculations of the Hessian to ensure that the optimized structures corresponds to the minima of the potentials energy surfaces (i.e., the absence of imaginary frequencies is indispensable). We observed that this is an important step to ensure the proper ground spin-state geometry for all the penta-coordinated species, especially for the **FePIm**. The out-of-plane displacement of the Fe-atoms is a very delicate entity and the optimization tends to converge into various local minima having a shorter out-of-plane displacement of the Fe atom. On the other hand for **FePImO2**, there are many closely spaced energy solutions with different Fe−O bond distances having negative stretching frequencies. These local minima appear along the reaction coordinate of the Fe−O bond formation rather than from the equilibrium Fe−O bonding situation.

dx.doi.org/10.1021/jp3021563 | *J. Phys. Chem. B* 2012, 116, 5849−5859

Table 1. Structural Parameters (in Å) of Optimized Geometries at the UB3LYP and GGA+U Levels[a]

species	Fe−N_p	Fe−N_m	Fe−L	O−O	ΔFe
FeP	2.01/2.01				0.0/0.0
	(1.97)[b]				(0.0)
FePCl	2.09/2.09		2.27/2.21		0.48/0.48
	(2.06)[c]		(2.22)[c]		(0.49)[c]
FePOH[d]	2.01/2.10		1.83/1.84		0.51/0.50
FePIm	2.11/2.09	2.19/2.22			0.43/0.32
	(2.09)[e]	(2.16)[e]			(0.42)[e]
FePImO_2	2.02/2.02	2.08/2.10	1.78/1.91	1.25/1.29	0.0/0.00
	(2.01)[f]	(2.06)[f]	(1.81)[f]	(1.24)[f]	(0.00)

[a]The observed experimental values are given in the parentheses, the first values before the oblique are obtained by UB3LYP. N_p indicates the pyrrolic nitrogens, N_m is the imidazole nitrogen, and L labels the ligand Cl or O. ΔFe is the out-of-plane displacement of the iron atom from the macrocyclic plane. [b]Reference 37. [c]Reference 38. [d]Crystallographic structure is not available. [e]Reference 39. [f]Reference 40.

Hence, analytical second derivative calculations are recommended for these types of systems. We also have optimized all the species in GGA (PW91)+U approach. The optimized molecular geometries are tabulated in Table 1.

The geometries are quite well reproduced both in the B3LYP and GGA+U approaches. The central Fe-atom in tetra-coordinated **FeP** and hexa-coordinated **FePImO2** are in-plane with the macro-molecular porphyrin rings. This is a nontrivial result for **FePImO2**, as the imidazole and O_2 ligands are different. The Fe−N_p distances are the same for both these systems with ∼2.00 Å bondlengths. In case of the high-spin ground state penta-coordinated systems (**FePOH**, **FePCl**, and **FePIm**) the Fe-atoms moves out-of-plane by about 0.4 to 0.5 Å. This was explained by the larger spatial atomic vloume of the Fe atom in the high-spin state as compared to the low-spin analog, which increases the strain inside the planar configuration and causes the out-of-plane displacement of the central metal atom. The high-spin also causes the weakening of the Fe−N_p bonds which eventually increase in the out-of-plane configurations.[20,41] However, a recent work by Walker et al.[42] contradicts these earlier explanations. From a quantum theory of atoms in molecule (QTAIM) analysis they observed that the atomic size for the high-spin Fe-atoms is smaller than that of the low-spin porphyrins. Also, they have predicted that the axial ligand plays the vital role in the out-of-plane displacements of the central metal atom.[42,43]

To perform a systematic assessment of the performance of various density functionals in calculations of spin-state energetics for these systems we have considered a range of density functionals. Here we have opted to perform localized basis sets calculations by choosing two GGA functionals, i.e., BLYP and PBE.[44−46] The GGA functionals depend on the LSDA density part and their reduced gradient. The natural development of the GGA functional is meta-GGA which includes the second derivatives of the electron density (the Laplacian). One of such mGGA functionals, Boese and Handy's τ-HCTH, is considered here.[47] In addition to GGA and meta-GGA functionals, four different hybrid-GGA functionals (B3LYP, PBE0, O3LYP, and X3LYP) are considered.[48,49] These hybrid functionals use different amounts of exact exchange, e.g., O3LYP (11.6%), B3LYP (20%), X3LYP (21.8%), and PBE0 (25%). The nonlocal correlation contributions (LYP) are same for the first three functionals although the local exchange and correlations contributions were parametrized slight differently. The hybrid PBE0 functional was constructed based on the PBE functional. A comparison of these functionals is expected to provide an insight into the dependence of the spin-state energetic on the nonlocal exact exchange.

Recently the M06 family functional based on meta-GGA by Truhlar and Zhao has attracted attention due to its success in the study of thermochemsitry, barrier heights, noncovalent interactions and bondings in transition metals.[50,51] In this work we have considered all the four functionals of M06 family. The M06-L is local functionals, while hybrid functional M06 and M06-2X contain 27% and 54% of exact HF exchange. The M06-HF contains 100% of HF-exchange. These functionals were parametric for the first and second row elements except M06-2X, which was not parametrized for the transition metal elements. The special part about the M06 functionals are the correlation functional. It treats the opposite-spin and parallel-spin correlations separately.The GGA+U functional which takes into account the on-site Hubbard-U Coulomb correlation corrections on top of the GGA is also consider for this work.[27,28]

III. SPIN STATES

The iron-porphyrin complexes with an even number of electrons in the d-orbitals have three lowest lying accessible spin-multiplets, i.e. singlet, triplet, and quintuplet, whereas for the odd-electron species the low-lying spin-states are doublet, quartet, and sextet. These spin-multiplets are generally referred to as the low, intermediate, and high spin states. Accurate evaluations of the ground state spin and the energies of the different spin-multiplets are an extremely difficult task. This issue has been addressed several times, but with little improvement especially regarding the XC-functionals. Here we will access the performance of various (hybrid) functionals, along with the GGA+U, in the following sequentially for each of the species.

1. Tetra-Coordinated FeP. The electronic structures and spin states of the two most popular species that are similar to tetra-coordinated iron porphyrin (**FeP**), the tetraphenylporphinato-iron(II) (FeTPP) and octaethylporphinato-iron(II) (FeOEP) have been investigated applying various experimental techniques. The ground state $S = 1$ with the electronic configuration $^3A_{2g}$ arising from the $d^2_{xy}d^2_{\pi}d^2_{z^2}$ configuration has been identified by Mössbauer,[37,52] magnetic,[53] and proton NMR[54,55] measurments on FeTPP. This assignment is in clear contrast with the resonance Raman assignment of ($^3E_{2g}$) that arises from a $d^2_{xy}d^3_{\pi}d^1_{z^2}$ electronic configuration.[56] A detailed analysis of various experimental data by Sontum et al.[57] doubted the previously assigned ground state ($^3E_{2g}$) for FeOEP. Kozlowski et al.,[19] applying the B3LYP functional, predicted the

dx.doi.org/10.1021/jp3021563 | J. Phys. Chem. B 2012, 116, 5849−5859

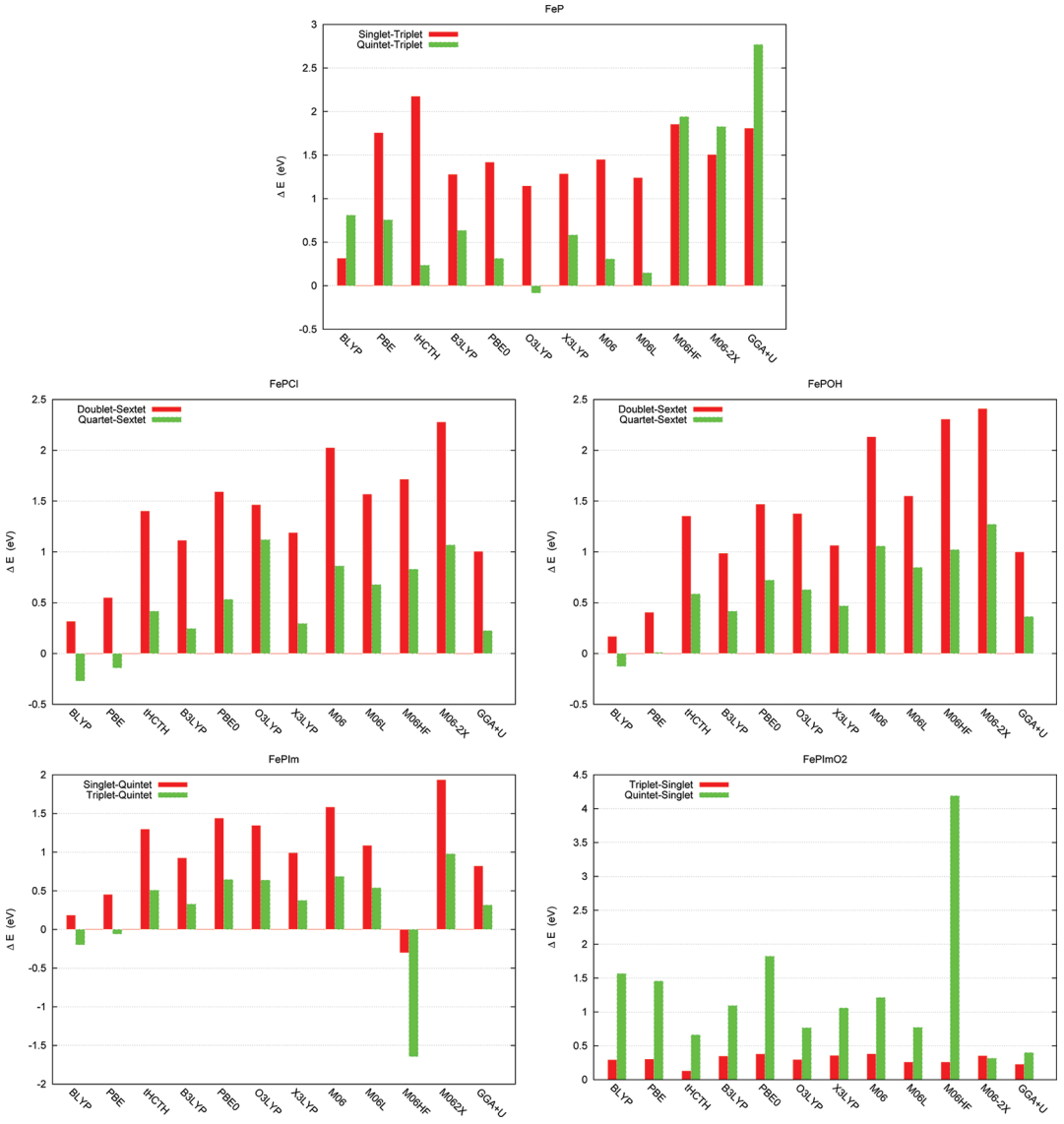

Figure 2. Relative energy of low-lying spin multiplets with respect to the ground-state energy is plotted for each of the investigated functionals. The reference spin multiplet is the triplet for **FeP**, the sextet for **FePCl**, **FePOH**, and **FePIm**, and the singlet for **FePImO2**. The energies of the singlet reference state for **FePImO2** are extracted from the broken-symmetry solution as $E_S = (E_B - aE_T)/(1-a)$, where $a = \langle S_B^2 \rangle /2$. The E_B, E_S, and E_T are the spin-contaminated broken-symmetry, spin-corrected singlet and triplet state energies, respectively.

correct ground state $^3A_{2g}$. A large number of follow-up calculations with various hybrid functionals reproduced the ground state triplet.[23,61] However, inconsistent answers are also noticeable in the literature of both wave function based as well as density-functional based approaches. The Hartree−Fock (HF) method wrongly predicted the $^5A_{1g}$ state as the ground state.[58] This failure was interpreted as being due to the lack of Coulomb electron correlation in HF. Initially, the complete active space self-consistent field reference wave function (CASPT2) calculations also failed to evaluate the ground spin-state accurately.[59,60] However, recently Vancoillie et al. have shown that when increasing the active space from (8, 11) to (16,15), the CASPT2 does provide $^3A_{2g}$. They have further applied the restricted active space method RASPT2 where different subspaces and excitation levels (RAS1 to RAS3) were chosen.[13,14] The RASPT2 (16,2,0; 4,11,0) provides accurate results similar to those of CASPT2(16,15) and the triplet state is the lowest energy state with low lying high-spin state. In all these calculations the geometry optimization was performed constraining the specific symmetry. Notably, these multi-configurational calculations provide the $^3A_{2g}$ ground-state configuration, the orbital occupation, $d^2_{x^2-y^2}d^2_{z^2}d^2_{\pi}d^0_{xy}$ is equivalent to the one that was obtained by Mössbauer, NMR, as well as DFT studies of Kozlowski et al. and Liao et al.[19,23]

The spin-state multiplet energies are sensitive to the applied functionals. A comparison of the various density functionals are given in Figure 2 for the species studied here. The experimentally observed ground state spin is $S = 1$ for **FeP**, $S = 5/2$ for **FePOH** and **FePCl**, $S = 2$ for **FePIm**, and $S = 0$ for **FePImO$_2$**. All the meta-GGA, hybrid-GGA and meta-hybid-GGA and GGA+U functionals considered in this work reproduced the ground spin-state accurately. However, the GGA functionals failed systematically in all these cases except for FeP and FePIm. Notably, even if the considered functional gives the correct ground state spin, the energy difference between the ground state spin multiplet and low-lying multiplets can vary quite significantly. This is illustrated in Figure 2 where these energy differences are given for the

dx.doi.org/10.1021/jp3021563 | J. Phys. Chem. B 2012, 116, 5849−5859

considered functionals. For **FeP** O3LYP predicts the quintet (S = 2) to be the ground state.

The GGA functionals BLYP and PBE both predicted the triplet ground state, however, the singlet lies below the quintet in case of the former functional whereas for the latter, the quintet lies below the singlet. The RASPT2 calculations by Vancoillie et al.[14] produced the energy difference ΔE_{Q-T} ($^5E_g-^3A_{2g}$) to be 0.21 eV and ΔE_{S-T} ($^1A_{2g}-^3A_{2g}$) to be 1.29 eV. The tHCTH functional produced the ΔE_{Q-T} much lower than the PBE, however, ΔE_{S-T} is much larger compared to the RASPT2 and to other hybrid functionals. The hybrid functionals (B3LYP, PBE0, X3LYP, O3LYP, and M06) and the local M06L all produced an identical ΔE_{S-T} energy gap in the range of 1.14−1.42 eV. But O3LYP wrongly produced the quintet as the ground state. The reason for this failure must be attributed to the Handy and Cohen's optimized local exchange part (OPTX), that was improved on B88X. The O3LYP is a hybrid functional that consist of 11.6% of nonlocal HF exchange and the same correlation functional of Lee-Young-Parr as in BLYP and B3LYP. The ΔE_{Q-T} calculated with the hybrid functionals and local M06-L are very small, only in the range of 0.14 (M06-L) to 0.63 (B3LYP) eV. Among the M06 family of functionals the M06 and M06-L produce a very close energy difference that is commensurate with the RASPT2 values by Vancoillie et al.[14] However, M06-L is a completely local functional. The functionals with excess nonlocal exchange M06-2X (54% HF) and M06HF (100% HF) have reversed the singlet and quintet's energy ordering. Here we observed that the functionals with a nonlocal exchange contribution from 20 to 27% are quite reliable for **FeP**. In case of GGA+U the singlet-quintet energy order has also changed, similar to the M06-2X and M06HF functionals. This might be attributed to an inadequate knowledge of the on-site Coulomb correlation U value. The linear-response evaluation of U might be helpful to determine the exact energy ordering applying GGA+U, especially for tetra coordinated porphyrins. The highly symmetric planar FeP species has several closely spaced electronic states with various possible electronic configurations for a particular spin-state and in addition, there are low-lying excited states which complicate the picture. This complicates the evaluation of the ground-state electronic structure of FeP in comparison to the other systems studied here.

2. Penta-Coordinated FePCl and FePOH. The penta-coordinated Fe(III)-porphyrin (**FePCl** and **FePOH**) have (formally) a d^5 electronic occupation and the central metal atom is displaced in such complexes from the plane of the porphyrin ring toward the axial ligands. Mössbaur spectra[62] and ESR spectra[63] have identified the high-spin sextet (S = 5/2) as the ground state. These systems are already being recognized as very challenging from the computational point of view, due to the subtle out-of-plane displacements of the central metal ion and the concomitant very shallow potential energy surface. Ghosh et al.[64,65] explored the **FePCl** explicitly applying DFT and wave function based quantum-chemical methods such as CCSD(T) and CASPT2. They initially observed that the PW91 exchange-correlation functional yields a quartet (S = 3/2) state being stable by 0.30 eV over the sextet (S = 5/2). Here we observed that the hybrid B3LYP and other hybrid functionals provide the sextet as the ground state. The CASPT2 calculations and CCSD(T) simulations on very small model systems were consistent with experiments, placing the sextet almost 0.73 eV below the quartet.[24,64,65] Here we find this energy difference for B3LYP to be 0.30 eV.

Liao et al. have investigated **FePCl** applying a wide range of exchange-correlation functionals. They observed that the highly parametrized HCTH/407, Becke00, B3LYP, B97, B97-1, and τ-HCTH-hyb are quite good to reproduce the experimentally observed ground spin-state.[61,66] They also observed that most of the GGA and meta-GGA functionals are biased toward the lower spin states, hence such functional fail to predict the high-spin ground state. In this respect, Hartree−Fock exchange favors the high-spin solution. Thus, the hybrid functionals are a good compromise between these to obtain the correct spin-states. In the present work we observed that the meta-GGA and other hybrid functionals correctly produce the experimentally observed ground-state spin, but the relative spin multiplet energies depend strongly on the functionals. However, the qualitative energy ordering of the spin multiplets remains largely the same and mostly independent of the choice of the functionals. Among the hybrid functionals B3LYP, PBE0, and X3LYP produced a low quartet-sextet energy difference of about 0.3 to 0.50 eV. The high quartet-sextet energy difference predicted by O3LYP is not unexpected, looking at its failure for **FeP**. Similarly, all the functionals belonging to the M06-family produced larger energy gaps. The reason of this larger gap appears to be overstabilization of the high-spin state systems (here ^{6}A state). Vancoillie et al. have also made similar observations.[13] The overstabilization of the high-spin states was noticed to be severe during the ^{7}A potential energy surface generation applying the M06/M06-2X functionals. This failure limited us to use the B3LYP functional in the PE surface calculation of the O_2 binding process. All the functionals result in a very low (in the range of 0.30−0.55 eV) quartet-sextet energy splitting, except for the O3LYP and M06-2X. The GGA +U approach is extremely competitive as compared to the results obtained by the comparatively expensive calculations of exact HF-exchange accounted by hybrid functionals. The GGA +U energy differences between the quartet-sextet is very close to that of the B3LYP and X3LYP functionals. The recently developed hybrid meta-GGA functional (M06-2X) increases the energy splittings of the spin multiplets for the penta-coordinated porphyrin systems.

3. Penta-Coordinated FePIm and Hexa-Coordinated FePImO2. The formal d-orbital occupation of **FePIm** and **FePImO2** is d^6; however, the electronic structure for the later is more complicated and will be addressed in the latter part of this section. The experimentally observed ground-state spins are the quintet and singlet, respectively. Hence, the oxygen adsorption/desorption is associate with the "spin-crossover" phenomenon.[4,8,67] The high spin (S = 2) deoxy-heme binds with the oxygen (S = 1) in paramagnetic state to form a low-spin (S = 0) oxy-heme. However, the complete mechanism of this versatile spin-crossover reaction, its energetics and reaction dynamics has not been understood completely.[20−22] The electronic structures of both of the complexes have been studied applying sophisticated quantum chemical methods, recently developed density functionals as well as in a hybrid QM and MM approach to systematically include the solvent effects.[68]

The quintet spin-state was obtained for the **FePIm**, although some inconsistent reports appeared in earlier literatures. We notice that the performances of the different hybrid functionals are quite similar, including the GGA+U. However, the M06-2X produced a large energy gap for the different spin multiplets. The best estimates for ΔE_{S-Q} and ΔE_{T-Q} for **FePIm** are in the range of 0.30−0.37 and 0.20−0.29 eV, respectively. These values were obtained by CASPT2 and CCSD(T)(∞).[12,13] Here

dx.doi.org/10.1021/jp3021563 | J. Phys. Chem. B 2012, 116, 5849−5859

we observe that the GGA functionals do provide improper ground states. However, all the other functionals except the M06-2X functional provided the quintet ground state. The ΔE_{S-Q} for B3LYP to M06-L are in the range of 0.92−1.50 eV and the ΔE_{T-Q} are in the range of 0.3−0.68 eV. The ΔE_{T-Q} as well as ΔE_{S-Q} values appear to be overestimated in comparison to the "best estimated" high-level wave function based quantum-chemistry calculations. However, a proper comparison of values would be more assuring when the calculations would have been performed with the same level of optimized geometry. The multireference character of the excited states for low and intermediate spin-state wave functions could be the major source of this overestimation when using the single Slater determinant approximation for the orbitals. Furthermore, the inclusion of the excess amount of HF-exchange in the M06 family worsens the spin-state energetics.

The calculation of the ground-state spin of **FePImO2** is a more complicated task due to the electron-transfer from the central metal to the axial O_2 ligand. Then, the closed-shell diamagnetic solutions are most likely to be obtained, instead of the open-shell singlet ground state which has been observed in various experiments.[68,69] However, the spin-symmetry broken solution preferably reproduces the open-shell singlet ground state for all GGA, meta-GGA approach. The energies of the different spin-multiplets can be extracted by a spin projection method suggested by Noodleman.[70] The relative spin-multiplet energies obtained by various DFT functionals for the **FePImO2** are plotted in Figure 2. The singlet ground state is reproduced unambiguously by all the functionals considered in this study. The ΔE_{Q-S} and ΔE_{T-S} energy differences for the hexa coordinated **FePImO$_2$** were estimated by Ribas-Arino et al.[82] applying CASPT2 (CASSCF), giving values that are 0.09 (0.11) and 0.14 (0.52) eV, respectively. The calculated ΔE_{Q-S} are in the range of 0.29 to 0.39 eV for the B3LYP to M06L functionals and also GGA+U. The ΔE_{T-S} energy difference are higher and computed to be in the range of 0.39 to 1.82 eV for the above-mentioned functionals.

The electronic structure of **FePImO2** and the chemical bonding between the Fe and O_2 molecule are very complicate in nature. There are various mechanisms that have been proposed, such as those due to Pauling, Weiss, and McClure-Goddard, to explain the observed magnetic properties, chemical bonding, and the spectroscopic properties of **FePImO2**. The Pauling picture suggested that the **FePIm** is in an $S = 0$ state, and that O_2 is also in $S = 0$ and that they interact diamagnetically.[71,72] The Weiss mechanism suggests that the **FePIm** transfers one electron to O_2 first and that the electrostatic interaction gives an interplay between $FePIm^+(S = 1/2)-O_2^-(S = 1/2)$.[73] The McClure-Goddard mechanism suggest that two unpaired electrons in the ferrous center pair up in a Heitler-London fashion, resulting in an antiferromagnetically bonded $FePIm(S = 1)-O_2^-$ $(S = 1)$ system.[74,75] A lucid discussion on the various bonding mechanisms and comparisons of the different theoretical calculations can be found in the work by Chen et al.[68] On the basis of valence bond (VB) analysis of the Kohn−Sham orbitals they observed that the $Fe(III)-O_2^-$ bonding is a complicated admixed picture of these three different mechanisms. The same conclusion was drawn by Jensen et al. on the basis of CASPT2 calculations.[76] The O_2 binding energies for **FePImO2** calculated for the optimized geometries (including the projected low spin energy corrections) are 6.02 and 4.82 kcal/mol for the B3LYP and M06 functionals, respectively. These calculated values are slightly better than the previous B3LYP calculation (3.8 kcal/mol).[12] The CASPT2[12] values are in the range of 4.1−9.9 kcal/mol while the experimentally obtained values are in the range of 10.1−13.3 kcal/mol.[77,78] The binding energy extracted from Figure 4 is 3.01 kcal/mol which lesser than the separately optimized cases.

IV. HEME AND O_2 INTERACTIONS

The oxygen binding process of the penta-coordinated **FePIm** is "spin-forbidden" and reversible in nature.[79−82] To understand this crucial "spin-crossover" phenomenon we have calculated the potential energy surface of the reaction in vacua by full optimization in the four different spin-states, except for fixing and manually varying the Fe−O redundant coordinate at the B3LYP level to obtain the reaction path. The consistent performance of the B3LYP functional in the calculation of molecular geometries, spin-state energetics, as well as O_2-binding energy favors this functional for the potential energy surface exploration. The hybrid M06 is a competitive functional, but due to the overstabilization of the high-spin state by the M06-family the $^7A_1$ state is made even lower in the O_2 bonded configurations. This rules out the possibility of using the M06 functionals in the evaluation of the potential energy curve. The study of the potential energy surface provides a completely new understanding of the oxygen-binding processes. In the fully optimized state the Fe−O bond length is 1.78 Å and directed along the molecular Cartesian z-axis. The evaluation of the potential energy surface (PES) for the oxygen binding process is very complicated because of its higher dimensional nature. So only varying the Fe−O distance will lead to an improper PES. However, an attempt was made to study a two-dimensional (Fe−O and Δd) potential energy surface by Nakashima et al.[81] They observed that the triplet ($^3A_1$) potential energy surface is dissociative in nature. Here we obtained a clear local minimum for the $^3A_1$ potential energy surface which was not identified previously in DFT (see Figure 4). The shape of the $^3A_1$-potential energy surface corresponds to that obtained in the recent CASPT2 calculations of Ribas-Arino et al.[82] However, and importantly, the global minima which we obtain is for the singlet ($^1A_1$) potential energy surface at 1.78 Å, which is in clear contrast to the work of Ribas-Arino et al., where they find the global minima in the triplet ($^3A_1$) potential energy surface.

The complete geometry relaxation fixing the internal distance between the Fe and O and manually varying the Fe−O distance will reduce the higher dimensional dependency of the PES into that of a one-dimensional variable. Applying this approach in the present work we observe that the in vacua potential energy surface provides a nonlinear dissociation/association reaction path for the O_2 (see Figure 3). This implies that the Fe−O reaction coordinate does not align exactly along the molecular z-axis. Notably, this was assumed to be the case in the previous studies.[80,82,83] Here we have computed the potential energy surface varying the Fe−O distances between 1.6 and 4.2 Å at intervals of 0.1 Å. The lowest energy point in the PES is obtained for the equilibrium Fe−O 1.78 Å. Above 3.5 Å the O_2 molecule lies completely flat on the porphyrin ring. In this situation there is no real chemical bonding observed between the porphyrin and O_2. This can be visualized through the nonoverlap of electron density on the O_2 and the **FePIm** shown in Figure 5 . The nonbonding interactions such as charge-dipole, dipole−induced dipole and van der Waals-type interactions must be operative in this case. This observation

dx.doi.org/10.1021/jp3021563 | J. Phys. Chem. B 2012, 116, 5849−5859

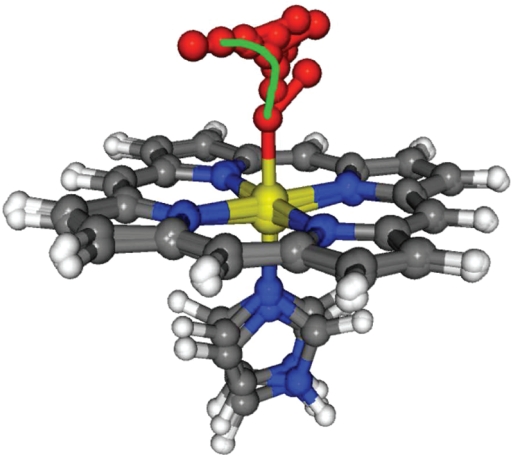

Figure 3. Comparison of the **FePImO2** optimized geometries where in each single calculation only the Fe−O distance is kept constant and all others are optimized. The Fe−O distance at the fully optimized geometry is 1.78 Å and Fe is in the macrocyclic plane. At a distance of 4.2 Å the O_2 becomes completely parallel to the porphyrin ring and the Fe has displaced out of the macrocyclic plane as in deoxy heme. The line indicates the approximate movement of the bonding O-atom along the reaction coordinate; this movement is not linear. This suggests that the O_2 binding with the deoxy-heme proceeds in a noncovalent manner first.

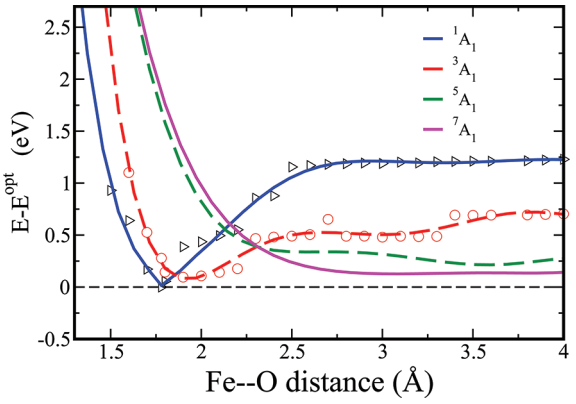

Figure 4. Calculated potential energy curves as a function of the Fe−O distance. These curve are obtained by (3rd order) polynomial fit of the single-point (SP) total energies obtain at 0.10 Å intervals. The original SP energies are shown as triangles and circles for the singlet and triplet states, respectively. At the optimized distance of 1.78 Å the singlet state (triangle) gives the (global) lowest point. This is not evident from from the fitted curve for the singlet. The spin-crossover from S = 3 to 1 occurs at ∼2.30 Å and from S = 1 to 0 at 1.85 Å.

indicates that during the association process the deoxy-heme and O_2 interactions are initiated through nonbonding interactions. These nonbonding interactions redistribute the π-electron density of the porphyrin, and in response to this redistribution of the electronic charges the out-of-plane displacement of the Fe-atom in the **FePIm** starts to reduce. It becomes completely planar at the equilibrium Fe−O distance (of 1.78 Å) in the singlet state. The decrease of the Fe−O distance, reduction of the out-of-plane Fe-atom displacement, and also the increase of the O−O bond length occur in a concerted manner.

The highest possible spin for the combined FePIm + O_2 system is S = 3 and the lowest spin is S = 0. Here we have explored the potential energy surfaces for all the possible spin states $^7A_1$ (S = 3), $^5A_1$ (S = 2), $^3A_1$ (S = 1), and $^1A_1$ (S = 0), However, in contrast to this in Figure 4. The lowest energy reaction path (blue full curve: up to 1.85 Å; red-dashed: from 1.85 to 2.30 Å) for the O_2 binding process has the unique feature of the "double spin-crossover" phenomenon. The first spin-crossover occurs at ∼2.3 Å. Above this distance both the **FePIm** and O_2 are in the HS state with the overall $^7A_1$ ground state (parallel alignment of **FePIm** and O_2 spins) and below this distance the triplet ($^3A_1$) becomes the ground state. The triplet was found to be globally the most stable state in the CASPT2 calculations by Ribas-Arino et al.[82] However, in contrast to this, here the singlet $^1A_1$ is obtained as the most stable state. The second spin-crossover point where a change from the triplet $^3A_1$ to the singlet $^1A_1$ state occurs, is observed at ∼1.85 Å Fe−O distance. Now there exists a clear overlap between the electron-density of **FePIm** and O_2 and the spin-density plots (discussed below) indicate an antiferromagnetic coupling between the **FePIm** and O_2. In the potential energy surface at 2.30 Å, although the triplet state is the ground state, the spin-density on the O_2 atoms belongs to the majority spin however a small coexistence of β-spin populations on the Fe atom is observed. The tiny overlap of the electron density occurs in this region (see Figure 5).

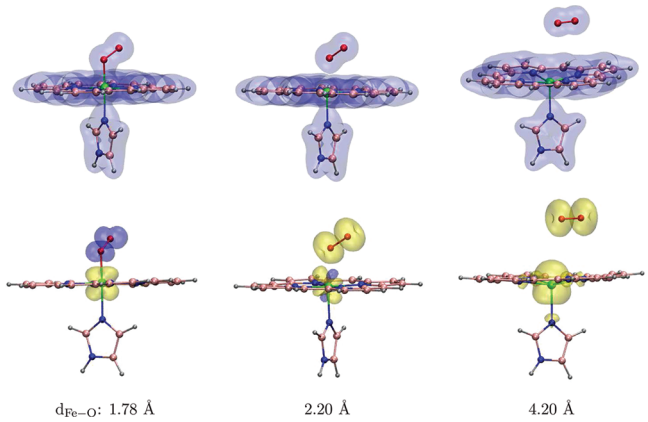

Figure 5. Calculated charge densities (top panels) and spin densities (bottom panels) for the FePIm-O_2 reaction for three distances along the reaction path. The three distances correspond to three different spin states: singlet $^1A_1$ at 1.78 Å, triplet $^3A_1$ at 2.30 Å, and septet $^7A_1$ state at 4.20 Å. The bright yellow isosurface depicts a dominantly majority-spin density, whereas dark blue depicts a dominantly minority-spin density.

The spin density plots in Figure 5 are in complete agreement with the appearance of the spin-crossover phenomenon in the potential energy curve. A closer look into the spin-density plots provides a crucial understanding on the spin-crossover mechanism. Above ∼2.30 Å the spins on Fe and O_2 belong to the majority spin (i.e., α-spin) and in the oxygenated complex the spin on the O_2 has flipped to the minority spin (i.e., β-spin). This spin-flipping occurs through an intra-atomic orbital spin polarization inside the central Fe-atom. As the Fe−O distance decreases below the first crossover point at ∼2.30 Å the Fe−O bond formation process starts because of the building up of β-spin on the Fe-atoms due to the atomic as well as orbital rearrangements. The smaller values of Mulliken atomic spin population on the Fe atom in the range of 1.85−

dx.doi.org/10.1021/jp3021563 | J. Phys. Chem. B 2012, 116, 5849−5859

Table 2. Calculated Natural Atomic (NA) Charges, Wiberg Bond-Index (BO), and Mulliken Spin Populations Obtained at the B3LYP/6-311+G(d,p) Level for the Selected Distances along the Fe−O Reaction Coordinate

	NA Charges			Wiberg's BO		Mulliken spin		
distance (Å)	Fe	O1	O2	Fe−O1	O1−O2	Fe	O1	O2
1.70	0.428	−0.075	−0.191	0.906	1.291	1.011	−0.264	−0.610
1.78	0.457	−0.104	−0.187	0.824	1.294	1.107	−0.330	−0.634
1.90	0.438	−0.069	−0.165	0.670	1.295	0.769	0.600	0.740
2.10	0.396	−0.003	−0.076	0.479	1.376	0.432	0.776	0.867
2.20	0.401	0.016	−0.045	0.398	1.408	0.327	0.829	0.905
2.40	0.990	−0.023	−0.040	0.232	1.422	4.270	0.870	0.923
2.80	1.000	0.020	−0.006	0.110	1.483	4.141	0.950	0.965
3.20	0.958	0.024	0.003	0.051	1.505	3.843	0.989	0.989
3.50	0.977	0.017	0.001	0.029	1.509	3.701	0.994	0.987
4.20	0.971	0.004	0.009	0.004	1.510	3.665	0.994	0.990

2.30 Å for the $^3A_1$-curve indicates this coexistence of the β-spin density (see Table 2).

The natural bond orbital and natural population analysis reveal that the natural atomic (NA) charges on the Fe atom has reduced in the oxygenated complex in comparison to the deoxy species. This happens because of the rearrangement of charge density which occurs within the macrocyclic porphyrin ring during the course of the reaction. There is approximately 0.5e electron density gained by the Fe atom due to the oxygen binding process and simultaneously the O_2 also gained ∼0.3e electron density. Hence this does not support the one electron transfer from Fe to O_2 (Weiss mechanism) as is generally reported in DFT. The transfer is better described as a one electron transfer from the macrocyclic porphyrin ring which is shared by the Fe−O bonded atoms. The Wiberg's bond order (BO) for the Fe−O and O−O provides snapshots of the bond formation during the binding process. From Table 2 it is clear that the Fe−O bond order is expectedly inversely correlated with the O−O bond order during the binding process. The decrease of O−O bond-order is associated with the population of π^*_{O2} orbitals.

To conclude, we find that the hybrid-DFT (B3LYP) functional indeed captures the subtle features of the potential energy surface in the oxygen binding process by heme and explains the intricate nature of the O_2 binding. The associative nature of the triplet $^3A_1$-curve is well reproduced. However, a second spin-crossover is observed to occur at short Fe−O reaction distances, giving the singlet as the true global minima. The Fe−O reaction coordinate is definitely nonlinear and the macrocyclic π-electron density plays an important role in the long-distance **FePIm** +O2 interactions. These hybrid-DFT calculations have hence captured the "spin-crossover" and "spin-flipping" mechanisms and provide the correct global minimum energy state.

V. MOLECULAR ORBITALS INTERPRETATION

The general consensus for the orbital occupations of metalloporphyrin systems is based on a pure atomic orbital picture for the pure metallic d-orbitals. This interprets adequately the orbital occupations and spin-states for the penta- and hexa-coordinated systems. However, due to the lack of the axial ligands in the tetra coordinated **FeP** and the coplanarity of the pyrrolic nitrogens and the central Fe atom, further complexity due to additional bonding is supplied. This will certainly lift the degeneracy of the atomic d-orbitals in the ligand field. From symmetry and orbital-occupation constrained DFT calculations for **FeP** by Liao et al.,[23,24] the energy ordering of the pure atomic-type d-orbitals were assigned to be the d^2_{xy} $d^2_{z^2}$ $d^2_{\pi^*}$. This configuration is similar to what was obtained in CASPT2 calculations by Vancoillie et al.[14] (only, they have chosen a slightly different reference axes system for the labeling of the d-orbitals than Liao et al.[23,24]). If this electronic configuration holds strictly true for the cases without any symmetry imposition, then there would be no peak corresponding to the $d_{x^2-y^2}$ orbital in the bonding region; however, it has a clear contribution in a few of the lowest molecular orbitals.[16,17] See also orbital 79A in Figure 5. Hence, the molecular orbitals picture provided by the spin-polarized GGA+U as well as hybrid-functional calculations present a more complex bonding scenario. The frontier molecular orbitals are hence found to be a result of a strong mixing of the pure metal orbitals with the ligand's π-orbitals. As a consequence, simple crystal field theory of splitting the degeneracy of the d-orbitals of the central metal atom in the presence of the ligand field of free-base porphyrin system cannot explain the peaks obtained in the LDOS of the plane wave calculation as well as hybrid functional calculations.

The span of the d-orbitals in the occupied region ranges from −6 eV up to the Fermi level. However the high-intensity d-orbitals (alpha and beta) peaks are positioned at around and above −3.0 eV (see Figure 5). This large span indicates that only the highest occupied Kohn−Sham orbitals are not solely responsible for the ground-state spin of the FeP. The LDOS clearly indicates a $S = 1$ ground state with one majority spin peak above the Fermi level and also three minority spin peaks above the Fermi level. It is also noticeable that the majority spin-peaks have splitted more than the expected five peaks. Whereas the minority spin-peaks consist of five nearly equally intense peaks. From the decomposition of the LDOS by projecting onto the individual atomic d-orbitals it is observed that the 3d orbitals mix strongly among themselves as well as with the macrocyclic π-orbitals especially the pyrrolic-N p-orbitals to form the MOs of the porphyrins. The ml-resolved DOS indicates a peak for the $d_{x^2-y^2}$ orbital at −5.0 eV. An inspection of the Kohn−Sham orbitals in the hybrid calculations also tells that the 79A (79A′) orbitals for alpha (beta) have a larger contribution of the $d_{x^2-y^2}$ also well below the Fermi level as is obtained by GGA+U. This indicates a partial occupation of the $d_{x^2-y^2}$ orbital which is the paradox. Taking a closer look on the orbitals, this paradox can be resolved from the bonding pictures with the crystal-field split orbitals. That is, the d-orbitals are first split according to the tetragonal ligand field of the free-base porphyrin. In this picture the energy of the $d_{x^2-y^2}$ orbital raises. This orbital will be empty if there is no further interaction possible and this will provide

dx.doi.org/10.1021/jp3021563 | J. Phys. Chem. B 2012, 116, 5849−5859

Table 3. Natural Atomic Orbital (NAO) Occupations for the Fe 3d Orbitals[a]

	alpha-orbitals					beta-orbitals				
	d_{xy}	d_{xz}	d_{yz}	$d_{x^2-y^2}$	d_{z2}	d_{xy}	d_{xz}	d_{yz}	$d_{x^2-y^2}$	d_{z^2}
FeP	0.984	0.969	0.969	0.341	0.975	0.984	0.969	0.052	0.261	0.0387
FePCl	0.978	0.977	0.974	0.976	0.983	0.312	0.193	0.192	0.038	0.347
FePOH	0.979	0.972	0.971	0.981	0.980	0.309	0.159	0.240	0.022	0.272
FePIm	0.983	0.962	0.964	0.979	0.984	0.833	0.046	0.188	0.179	0.113
FePImO2	0.985	0.979	0.976	0.978	0.983	0.957	0.807	0.470	0.323	0.356

[a]The alpha and beta-electrons are provided separately.

the configuration as given by Liao et al.[23] However the orbital lobes are directed to the four pyrrolic-N atoms, and each of the N atoms contains a p_z electron which contributes in the macrocyclic aromaticity of the porphyrins. The planarity of FeP molecules highly favors the mixing of the occupied four p_z-orbitals on N-atoms with the vacant $d_{x^2-y^2}$ orbital on the Fe-atom. This is the d_π-p_π back bonding, which is responsible for the observed $d_{x^2-y^2}$ peaks in the bonding regions. The considerable amount of $d_{x^2-y^2}$ population in Table 3 by α and β-electrons supports the back-bonding and also justify its low-lying nature. We also observe that the d_{xz} (83A) and d_{yz} (86A) have been shifted down in the bonding regions in case of majority spin whereas these remain in the frontier orbitals for the minority spins. In a simple crystal field concept, these orbitals should however be degenerate. But neither GGA+U nor any hybrid-functional calculation indicates a degeneracy of the d_{xz} and d_{yz} orbitals.

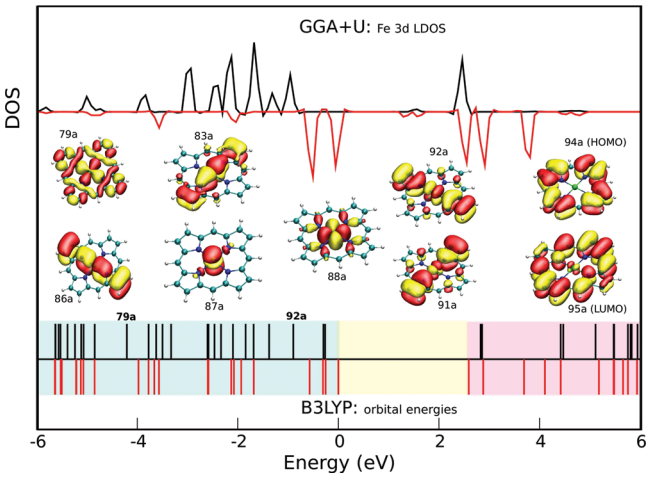

Figure 6. Orbital energy levels obtained by B3LYP for FeP are shown in the lower plot, and the Fe-3d local density of state (LDOS) obtained from GGA+U calculations is shown in the upper plot. The LDOS were corrected by the Fermi energy levels and the B3LYP Kohn–Sham energy spectrum was corrected by setting the beta-HOMO at 0 eV.

The natural atomic spin–orbital population analysis have been performed for the species on respective B3LYP density matrix and the alpha and beta orbitals occupations are provided in Table 3. The NAO population coincide with observed fact of back-bonding in the canonical Kohn–Sham orbitals. The $d_{x^2-y^2}$ has considerable alpha and beta electron occupations whereas the d_{z2} orbital is singly populated for **FeP**. In the case of **FePCl** and **FePOH** all the five α-orbitals are singly occupied, however there are small amount of β-occupations must be due to the ligand–metal charge transfer. The d-orbital population for the **FePIm** is well reflected as well as for **FePIm**. However the high β-orbitals occupation for the d_{xz}, d_{yz}, and d_{z^2} due to the axial O2 binding and due to achieved planarity the $d_{x^2-y^2}$ orbital is also expected to be slightly populated.

VI. CONCLUSIONS

In summary, we have investigated the performance of various GGA, hybrid-GGA, and meta-hybrid GGA functions to investigate the spin-state, spin-multiplet energy splittings, and geometrical parameters for five heme-related porphyrin complexes. The experimental observed ground spin-state for all the species could accurately be reproduced with all the hybrid functionals including M06 as well as with the GGA+U functional. The spin-state energetic obtained by the M06 and M06-L are consistent with other hybrid functionals. However, the inclusion of excess HF in the M06-family do not help. B3LYP describes spin states correctly, however it underestimates the O_2-binding energy. Performing a detailed assessment of the recently developed functionals we have studied the spin-crossover oxygen addition reaction with FePIm. This provides a completely new understanding of the Fe–O reaction coordinate for the in vacua case. However, this cannot be directly compared with the in vivo mechanism of the oxygen addition to hemoglobin, where the surrounding proteins and the distant histidine may also play a vital role. In the protein the rotation of the prosthetic histidine group is also restricted. Finally, the metal–ligand bonding for the tetra-coordinated porphyrin system is investigated. Unoccupied $d_{x^2-y^2}$ orbitals were previously predicted from orbital occupation constraint density functional theory[23] whereas recently the CASPT2 predicted their double occupancy.[14] However, the site-specific LDOS for the Fe-3d ion shows a contribution from this Fe-3d orbitals far below the Fermi energy and in the bonding region. This has been understood as the back-donation from the occupied π-orbital from the macrocyclic ligand to the unoccupied $d_{x^2-y^2}$ orbital.

AUTHOR INFORMATION

Corresponding Author

*E-mail: ehesan.ali@theochem.rub.de.

Notes

The authors declare no competing financial interest.

ACKNOWLEDGMENTS

This work has been supported by the Swedish Research Council (VR), the Swedish International Development Cooperation Agency (SIDA), the European Community through FP6 MOTTEST, the C. Tryggers Foundation, and the Swedish National Infrastructure for Computing (SNIC).

REFERENCES

(1) Nam, W. *Acc. Chem. Res.* **2007**, *40*, 522−531.
(2) Denisov, I. G.; Makris, T. M.; Sligar, S. G.; Schlichting, I. *Chem. Rev.* **2005**, *105*, 2253−2277.
(3) Meunier, B.; de Visser, S. P.; Shaik, S. *Chem. Rev.* **2004**, *104*, 3947−3980.
(4) Gütlich, P.; Garcia, Y.; Woike, T. *Coord. Chem. Rev.* **2001**, *219*, 839−879.
(5) Wittenberg, J. B.; Wittenberg, B. A.; Peisach, J.; Blumberg, W. E. *Proc. Natl. Acad. Sci.* **1970**, *67*, 1846−1853.
(6) Caughey, W. S.; Smith, G. A.; O'Keeffe, D. H.; Maskasky, J. E.; Smith, M. I. *J. Biol. Chem.* **1975**, *250*, 7602−7622.
(7) Wernsdorfer, W.; Aliaga-Alcalde, N.; Hendrickson, D. N.; Christou, G. *Nature* **2002**, *416*, 406409.
(8) Wäckerlin, C.; Chylarecka, D.; Kleibert, A.; Müller, K.; Iacovita, C.; Nolting, F.; Jung, T. A.; Ballav, N. *Nat. Commun.* **2010**, *1*, 61.
(9) Bernien, M.; Miguel, J.; Weis, C.; Ali, Md. E.; Kurde, J.; Krumme, B.; Panchmatia, P. M.; Sanyal, B.; Piantek, M.; Srivastava, P.; Baberschke, K.; Oppeneer, P. M.; Eriksson, O.; Kuch, W.; Wende, H. *Phys. Rev. Lett.* **2009**, *102*, 047202.
(10) Ali, Md. E.; Sanyal, B.; Oppeneer, P. M. *J. Phys. Chem. C* **2009**, *113*, 14381−14383.
(11) Petit, L.; Quartarolo, A.; Adamo, C.; Russo, N. *J. Phys. Chem. B* **2006**, *110*, 2398−2404.
(12) Radoń, M.; Pierloot, K. *J. Phys. Chem. A* **2008**, *112*, 11824−11832.
(13) Vancoillie, S.; Zhao, H.; Radoń, M.; Pierloot, K. *J. Chem. Theo. Comput.* **2010**, *6*, 576−582.
(14) Vancoillie, S.; Zhao, H.; Tran, V. T.; Hendrickx, M. F. A.; Pierloot, K. *J. Chem. Theo. Comput.* **2011**, *7*, 3961−3977.
(15) Liao, M.; Huang, M.; Watts, J. *J. Phys. Chem. A* **2010**, *114*, 9554−9569.
(16) Panchmatia, P. M.; Sanyal, B.; Oppeneer, P. M. *Chem. Phys.* **2008**, *343*, 47−60.
(17) Panchmatia, P. M.; Ali, Md. E.; Sanyal, B.; Oppeneer, P. M. *J. Phys. Chem. A* **2010**, *114*, 13381−13387.
(18) Oppeneer, P. M.; Panchmatia, P. M.; Sanyal, B.; Eriksson, O.; Ali, Md. E. *Prog. Surf. Sci.* **2009**, *84*, 18−29.
(19) Kozlowski, P.; Spiro, T.; Berces, A. *J. Phys. Chem. B* **1998**, *102*, 2603−2608.
(20) Rovira, C.; Kunc, K.; Hutter, J.; Parrinello, M. *J. Phys. Chem. A* **1997**, *101*, 8914−8925.
(21) Rovira, C.; Parrinello, M. *Intl. J. Quant. Chem.* **2000**, *80*, 1174−1180.
(22) Rovira, C.; Kunc, K.; Hutter, J.; Parrinello, M. *Inorg. Chem.* **2001**, *40*, 11−7.
(23) Liao, M. S.; Scheiner, S. *J. Comput. Chem.* **2002**, *23*, 1391−1403.
(24) Liao, M. S.; Scheiner, S. *J. Chem. Phys.* **2002**, *116*, 3635−3645.
(25) Kümmel, S.; Kronik, L. *Rev. Mod. Phys.* **2008**, *80*, 3−60.
(26) Marom, N.; Kronik, L. *Appl. Phys. A: Mater. Sci. Process.* **2009**, *95*, 159−163.
(27) Anisimov, V. I.; Aryasetiawan, F.; Lichtenstein, A. I. *J. Phys.: Condens. Matter* **1997**, *9*, 767−808.
(28) Anisimov, V. I.; Solovyev, I. V.; Korotin, M. A.; Czyzyk, M. T.; Sawatzky, G. A. *Phys. Rev. B* **1993**, *48*, 16929−16934.
(29) Perdew, J. P.; Zunger, A. *Phys. Rev. B* **1981**, *23*, 5048−5079.
(30) Cremer, D.; Filatov, M.; Polo, V.; Kraka, E.; Shaik, S. *Int. J. Mol. Sci.* **2002**, *3*, 604−638.
(31) Hay, P. J.; Wadt, W. R. *J. Chem. Phys.* **1985**, *82*, 270−283.
(32) Frisch, M. J.; Trucks, G. W.; Schlegel, H. B.; Scuseria, G. E.; Robb, M. A.; Cheeseman, J. R.; Scalmani, G.; Barone, V.; Mennucci, B.; Petersson, G. A.; Nakatsuji, H.; Caricato, M.; Li, X.; Hratchian, H. P.; Izmaylov, A. F.; Bloino, J.; Zheng, G.; Sonnenberg, J. L.; Hada, M.; Ehara, M.; Toyota, K.; Fukuda, R.; Hasegawa, J.; Ishida, M.; Nakajima, T.; Honda, Y.; Kitao, O.; Nakai, H.; Vreven, T.; Montgomery, Jr., J. A.; Peralta, J. E.; Ogliaro, F.; Bearpark, M.; Heyd, J. J.; Brothers, E.; Kudin, K. N.; Staroverov, V. N.; Kobayashi, R.; Normand, J.; Raghavachari, K.; Rendell, A.; Burant, J. C.; Iyengar, S. S.; Tomasi, J.; Cossi, M.; Rega, N.; Millam, N. J.; Klene, M.; Knox, J. E.; Cross, J. B.; Bakken, V.; Adamo, C.; Jaramillo, J.; Gomperts, R.; Stratmann, R. E.; Yazyev, O.; Austin, A. J.; Cammi, R.; Pomelli, C.; Ochterski, J. W.; Martin, R. L.; Morokuma, K.; Zakrzewski, V. G.; Voth, G. A.; Salvador, P.; Dannenberg, J. J.; Dapprich, S.; Daniels, A. D.; Farkas, .; Foresman, J. B.; Ortiz, J. V.; Cioslowski, J.; Fox, D. J. *Gaussian 09*, revision A.1; Gaussian, Inc.: Wallingford, CT, 2009.
(33) Blöchl, P. E. *Phys. Rev. B* **1994**, *50*, 17953.
(34) Perdew, J. P.; Wang, Y. *Phys. Rev. B* **1992**, *45*, 13244.
(35) Kresse, G; Hafner, J. *Phys. Rev. B* **2008**, *47*, R558.
(36) Kresse, G; Furthmüller, J. *Phys. Rev. B* **1996**, *54*, 11169.
(37) Collman, J. P.; Hoard, J. L.; Kim, N.; Lang, G.; Reed, C. A. *J. Am. Chem. Soc.* **1975**, *97*, 2676−2681.
(38) Scheidt, W. R.; Finnegan, M. G. *Acta. Crystallogr. Sect. C* **1989**, *45*, 1214−1216.
(39) Vojtechovsky, J.; Chu, K.; Berendzen, J.; Sweet, R. M.; Schlichting, I. *Biophys. J.* **1999**, *77*, 2153−2174.
(40) Unno, M.; Chen, H.; Kusama, S.; Shaik, S.; Ikeda-Saito, M. *J. Am. Chem. Soc.* **2007**, *129*, 13394−13395.
(41) Dunietz, B. D.; Dreuw, A.; Head-Gordon, M. *J. Phys. Chem. B* **2003**, *107*, 5623.
(42) Walker, V. E. J.; Castillo, N.; Matta, C. F.; Boyd, R. J. *J. Phys. Chem. A* **2010**, *114*, 10315−10319.
(43) Ugalde, J. M.; Dunietz, B.; Dreuw, A.; Head-Gordon, M.; Boyd, R. J. *J. Phys. Chem. A* **2004**, *108*, 4653−4657.
(44) Becke, A. *Phys. Rev. A* **1988**, *38*, 3098−3100.
(45) Perdew, J.; Burke, K.; Ernzerhof, M. *Phys. Rev. Lett.* **1996**, *77*, 3865−3868.
(46) Lee, C.; Yang, W.; Parr, R. G. *Phys. Rev. B* **1988**, *37*, 785−789.
(47) Boese, A. D.; Handy, N. C. *J. Chem. Phys.* **2002**, *116*, 9559−9569.
(48) Becke, A. *J. Chem. Phys.* **1993**, *98*, 1372−1377.
(49) Hoe, W.; Cohen, A.; Handy, N. *Chem. Phys. Lett.* **2001**, *341*, 319−328.
(50) Zhao, Y.; Truhlar, D. *Theo. Chem. Acc.* **2008**, *120*, 215−241.
(51) Zhao, Y.; Schultz, N.; Truhlar, D. *J. Chem. Theory. Comput.* **2006**, *2*, 364−382.
(52) Lang, G.; Spartalian, K.; Reed, C. A.; Collman, J. P. *J. Chem. Phys.* **1978**, *69*, 5424−5427.
(53) Boyd, P.; Buckingham, D.; McMeeking, R.; Mitra, S. *Inorg. Chem.* **1979**, *18*, 3585−3591.
(54) Goff, H.; Lamar, G. *J. Am. Chem. Soc.* **1977**, *99*, 6599−6606.
(55) Mispelter, J.; Momenteau, M.; Lohste, J. *J. Chem. Phys.* **1980**, *72*, 1003−1012.
(56) Kitagawa, T.; Teraoka, J. *Chem. Phys. Lett.* **1979**, *63*, 443−446.
(57) Sontum, S.; Case, D.; Karplus, M. *J. Chem. Phys.* **1983**, *79*, 2881−2892.
(58) Scherlis, D. A.; Estrin, D. A. *Int. J. Quantum Chem.* **2002**, *87*, 158−166.
(59) Choe, Y.; Nakajima, T.; Hirao, K.; Lindh, R. *J. Chem. Phys.* **1999**, *111*, 3837−3845.
(60) Pierloot, K. *Mol. Phys.* **2003**, *101*, 2083−2094.
(61) Liao, M. S.; Watts, J.; Huang, M. *J. Comput. Chem.* **2006**, *27*, 1577−1592.
(62) Dolphin, D. H.; Sams, J. R.; Tsin, T. B.; Wong, K. L. *J. Am. Chem. Soc.* **1978**, *100*, 1711−1718.
(63) Marathe, V.; Mitra, S. *J. Chem. Phys.* **1983**, *78*, 915−920.
(64) Ghosh, A.; Taylor, P. *Curr. Opin. Chem. Biolg.* **2003**, *7*, 113−124.
(65) Ghosh, A. *J. Biol. Inorg. Chem.* **2006**, *11*, 712−724.
(66) Liao, M.; Watts, J.; Huang, M. *J. Phys. Chem. A* **2007**, *111*, 5927−5935.
(67) Gaspar, A. B.; Seredyuk, M.; Gütlich, P. *Coord. Chem. Rev.* **2009**, *253*, 2399−2413.
(68) Chen, H.; Ikeda-Saito, M.; Shaik, S. *J. Am. Chem. Soc.* **2008**, *130*, 14778−14790.
(69) Chen, H.; Lai W. Yao, J.; Shaik, S. *J. Chem. Theory Comput.*. **2011**, *7*, 3049−3053.
(70) Noodleman, L. *J. Chem. Phys.* **1981**, *74*, 5737−5743.
(71) Pauling, L.; Coryell, C. D. *Proc. Natl. Acad. Sci.* **1936**, *22*, 210−216.

(72) Pauling, L. *Nature* **1964**, *203*, 182−183.
(73) Weiss, J. J. *Nature* **1964**, *202*, 83−84.
(74) McClure, D. S. *Radiation. Res. Suppl.* **1960**, *2*, 218−224.
(75) Goddard, W. A., III; Olafson, B. D. *Proc. Natl. Acad. Sci.* **1975**, *72*, 2335−2339.
(76) Jensen, K. P.; Roos, B. O.; Ryde, U. *J. Inorg. Biochem.* **2005**, *99*, 45−54.
(77) Blomberg, L. M.; Blomberg, M. R.; Siegbahn, P. E. J. *Inorg. Biochem.* **2005**, *99*, 949−958.
(78) Olson, J. C.; Phillips, G. N. J. *Biol. Inorg. Chem.* **1997**, *2*, 544−552.
(79) Scherlis, D. A.; Cococcioni, M.; Sit, P.; Marzari, N. *J. Phys. Chem. B* **2007**, *111*, 7384−7391.
(80) Jensen, K. P.; Ryde, U. *J. Biol. Chem.* **2004**, *279*, 14561−14569.
(81) Nakashima, H.; Hasegawa, J. Y.; Nakatsuji, H. *J. Comput. Chem.* **2006**, *27*, 426−433.
(82) Ribas-Arino, J.; Novoa, J. J. *Chem. Commun.* **2007**, *30*, 3160−3162.
(83) Sun, Y.; Hu, X.; Li, H.; Jalbout, A. F. *J. Phys. Chem. C* **2009**, *113*, 14316−14323.